Article

Synthesis, Characterization, and Evaluation of Antifungal Activity of 1-Butyl-3-hexyl-1*H*-imidazol-2(3*H*)-selenone by Surface-Enhanced Raman Spectroscopy

Noor ul Huda,[#] Muhammad Wasim,[#] Haq Nawaz,* Muhammad Irfan Majeed,* Muhammad Rizwan Javed, Nosheen Rashid,* Muhammad Adnan Iqbal, Anam Tariq, Ahmad Hassan, Muhammad Waseem Akram, Faisal Jamil, and Muhammad Imran

Read Online

ACCESS | 📊 Metrics & More | 📖 Article Recommendations | 🆘 Supporting Information

ABSTRACT: In the present research work, a selenium N-heterocyclic carbene (Se−NHC) complex/adduct was synthesized and characterized by using different analytical methods including FT-IR, ^{1}HNMR, and ^{13}CNMR. The antifungal activity of the Se−NHC complex against *Aspergillus flavus* (*A. flavus*) fungus was investigated with disc diffusion assay. Moreover, the biochemical changes occurring in this fungus due to exposure of different concentrations of the in-house synthesized compound are characterized by surface-enhanced Raman spectroscopy (SERS) and are illustrated in the form of SERS spectral peaks. SERS analysis yields valuable information about the probable mechanisms responsible for the antifungal effects of the Se−NHC complex. As demonstrated by the SERS spectra, this Se−NHC complex caused denaturation and conformational changes in the proteins as well as decomposition of the fungal cell membrane. The SERS spectra were analyzed using two chemometric tools such as principal component analysis (PCA) and partial least-squares discriminant analysis (PLS-DA). The fungal samples' SERS spectra were differentiated using PCA, while various groups of spectra were discriminated with ultrahigh sensitivity (98%), high specificity (99.7%), accuracy (100%), and area under the receiver operating characteristic curve (87%) using PLS-DA.
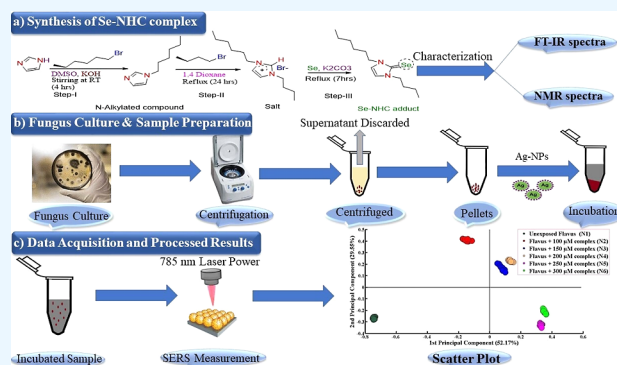
1. INTRODUCTION

Invasive fungal infections potentially cause 1.7 million deaths every year.[1] The mortality rate caused by fungal infections is greater than that of other diseases such as tuberculosis and malaria.[2] About 300 species out of 5 million known fungal species are reported to cause illness, allergy, and toxicity in humans. These fungal species belong to one of the five major genera which include *Candida* (*Candida albicans*, *Candida glabrata*, *Candida krusei*, *Candida parapsilosis*, *Candida tropicalis*, *Candida kefyr*, and *Candida guilliermondii*), *Aspergillus* (*Aspergillus flavus*, *Aspergillus niger*, and *Aspergillus fumigatus*), *Cryptococcus* (*Cryptococcus neoformans*), *Fusarium* (*Fusarium oxysporum*, *Fusarium moniliforme*, and *Fusarium solani*) and *Pneumocystis*.[3]

Fungal infections can be extensively treated by antifungal drugs that cause very low or no toxicity to the host organisms. For the treatment of fungal infections in humans, five major antifungal classes have been used such as azoles, polyenes, allylamines, pyrimidines, and echinocandins.[4,5] Overuse of these valuable substances results into enhanced antimicrobial resistance, leaving some infections untreated.[6] Organometallic-based antibacterial and antifungal drugs have been developed

as some of the organometallic compounds when coordinated with metal ions have great antibacterial and antifungal activities.[7]

Selenium-based N-heterocyclic carbene complexes have been used as suitable drug candidates for the cancer, bacterial, and fungal infections.[8] Selenium, an antioxidant, can be used for the treatment of chronic metabolic diseases, such as dyslipidemia, hyperglycemia, hyperphenylalaninemia, diabetes, arteriosclerosis, and phenylketonuria.[9] Selenium compounds can also be used as chemotherapeutic agents because of their high anticancer activity and low toxicity.[10] Selenium, in trace amount, can be used as an antibacterial agent and antifungal agent, making it suitable for medicinal purpose.[11]

Many methods including disk and well diffusion methods, growth inhibition by broth dilution tests, bioautography, and

radial growth inhibition methods are available that allow the analysis of the antifungal activity of any antifungal drug. These methods are used to measure the minimum fungicidal concentration value that corresponds to the minimum concentration of an antifungal agent that avoids further growth of the microorganism. Nevertheless, it is important to note that these methods have their own limitations, including their high cost, labor-intensive nature, and time-consuming process.[12−14] In order to overcome these limitations, the development of fast, cost-effective, and noninvasive methods is mandatory.

However, Raman spectroscopy (RS) is proficient in overcoming the abovementioned limitations. It is based on the idea of inelastic scattering which is widely used for the characterization of pharmaceutical formulations, analysis of the interaction of drug candidates with various microorganisms,[15] elaboration of kinetic processes in delivery of therapeutic agents, as well as for disease diagnosis.[16] RS can be employed on biological systems to obtain spectra that act as fingerprint even for the smallest species.[17]

Surface-enhanced Raman scattering (SERS) is the modified form of RS by employing nanoparticles (NPs) that significantly results into the improved signal-to-noise ratio up to 10^8 in Raman measurements.[18] "Raman indicator" is the recent development in the SERS domains for the ultrasensitive detection of protein and molecular imprinting.[19,20]

Metallic nanoparticles, such as silver nanoparticles (Ag-NPs), have been widely used as the SERS substrate because they exhibit strong surface plasmon resonance (SPR) effect that ultimately leads to the strong SERS enhancement factor almost $10^{10}-10^{11}$.[21,22] In the current study, Ag-NPs are preferred as the SERS substrate to improve the Raman signal because these nanoparticles show the stronger SPR effect due to the presence of greater number of active sites that would lead to create more "hot spots", resulting in the SERS enhancement factor even greater than that of the Au-NPs.[23,24] Ag-NPs are convenient to prepare, inexpensive, exhibit greater extinction coefficients, and possess more ratio of scattering to extinction.[25]

In the current study, SERS analysis along with chemometric analytical techniques, principal component analysis (PCA), and partial least-squares discriminant analysis (PLS-DA) is carried out to compare the SERS spectral features of *A. flavus*, exposed to the selenium-based organometallic compound with that of unexposed *A. flavus*. The differentiation between SERS features of these two classes are analyzed by comparing their mean plots and scatter score plots. These differentiating spectral features help us understand the occurrence of biochemical variations in the fungal strain due to the exposure of selenium N-heterocyclic carbene (Se−NHC) complex and the mode of action of this antifungal agent. A thorough investigation of the literature demonstrated that this work has not yet been published.

2. RESULTS AND DISCUSSION

2.1. FT-IR Spectral Analysis. Synthesis of the Se−NHC adduct was accomplished in three independent steps by following the procedure published recently.[26] Very short-ranged peaks (3500−500 cm^{-1}) are observed in the experimental FT-IR spectra, as demonstrated in Figure 1. Below 3000 cm^{-1}, a peak of C−H stretching is observed. Higher and lower frequency peaks are due to symmetric and antisymmetric C−H stretching. Stretching vibrations of C−C are observed between 1200 and 1750 cm^{-1}, and C−C bending
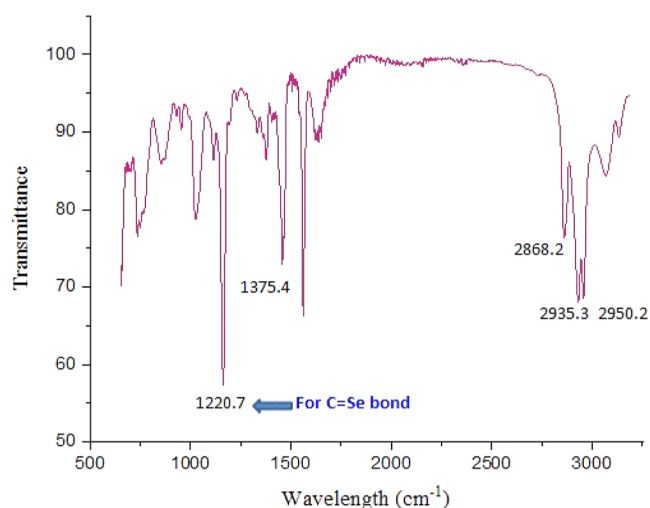

Figure 1. FT-IR spectra of the Se−NHC adduct.

vibration is found below 500 cm^{-1}. Bending vibrations of CH$_3$ and CH$_2$ are observed at 1131 and 1375 cm^{-1}, respectively.[26]

A particular pattern in the FT-IR spectra was observed between 1460 and 1100 cm^{-1} that might be due to fundamental vibrational frequency of the carbon selenium (C=Se) bond. The similar behavior was confirmed by literature reflecting the vibrational frequency for the carbon selenium bond of imidiazolium adducts at 1222 cm^{-1}.[27] This specific peak is also evident in Figure 1, showing the FT-IR spectra of the Se−NHC-based product.

2.2. NMR Spectral Analysis. The main feature in ^{1}H NMR spectra during analysis of NHC salt was a peculiar peak observed at 8−10 ppm, which corresponds to the resonance frequency of the acidic proton of carbene carbon. This resonance frequency is characteristic of carbene proton. As NHC salt had been successfully converted into the selenium adduct, the acidic proton peak was absent in Se−NHC adduct proton NMR spectra. A similar pattern is also reported in the literature which showed disappearance of the resonance frequency of the carbene proton peak as an indication of successful conversion of NHC salt into the selenium adduct.[28,29] Similar substantial evidence was also observed through ^{13}C NMR spectroscopy for successful synthesis of the designed NHC salt. Prominent feature of resonance frequency of carbene carbon was observed for the synthesized selenium adduct at 154.8 ppm.

Figure 2a,b shows ^{1}H NMR spectra and ^{13}C NMR spectra of Se−NHC complex/adduct, respectively. ^{1}H NMR spectra and ^{13}C NMR spectra of Se−NHC ligand/salt have been added in the Supporting Information as Figure S1a,b. Proton NMR spectra of the NHC ligand/salt (Figure S1a) reflect that a peak of acidic proton is prominent at 9.20 ppm, and this peak disappears in the Se−NHC adduct in Figure 2a. Similarly, in ^{13}C NMR spectra of the NHC salt, the NCN peak appears at 135.9 (Figure S1b), and this peak shifted toward downfield region 154.8 ppm, as shown in Figure 2b, which is an indication of successful incorporation of selenium and formation of the complex.

2.3. Chemical Structure of 1-Butyl-3-hexyl-1H-imidazol-2(3H)-selenone. Selenium, an antioxidant, can be used for the treatment of chronic metabolic problems, such as dyslipidemia, hyperglycemia, hyperphenylalaninemia, diabetes, arteriosclerosis, and phenylketonuria.[9] Selenium compounds
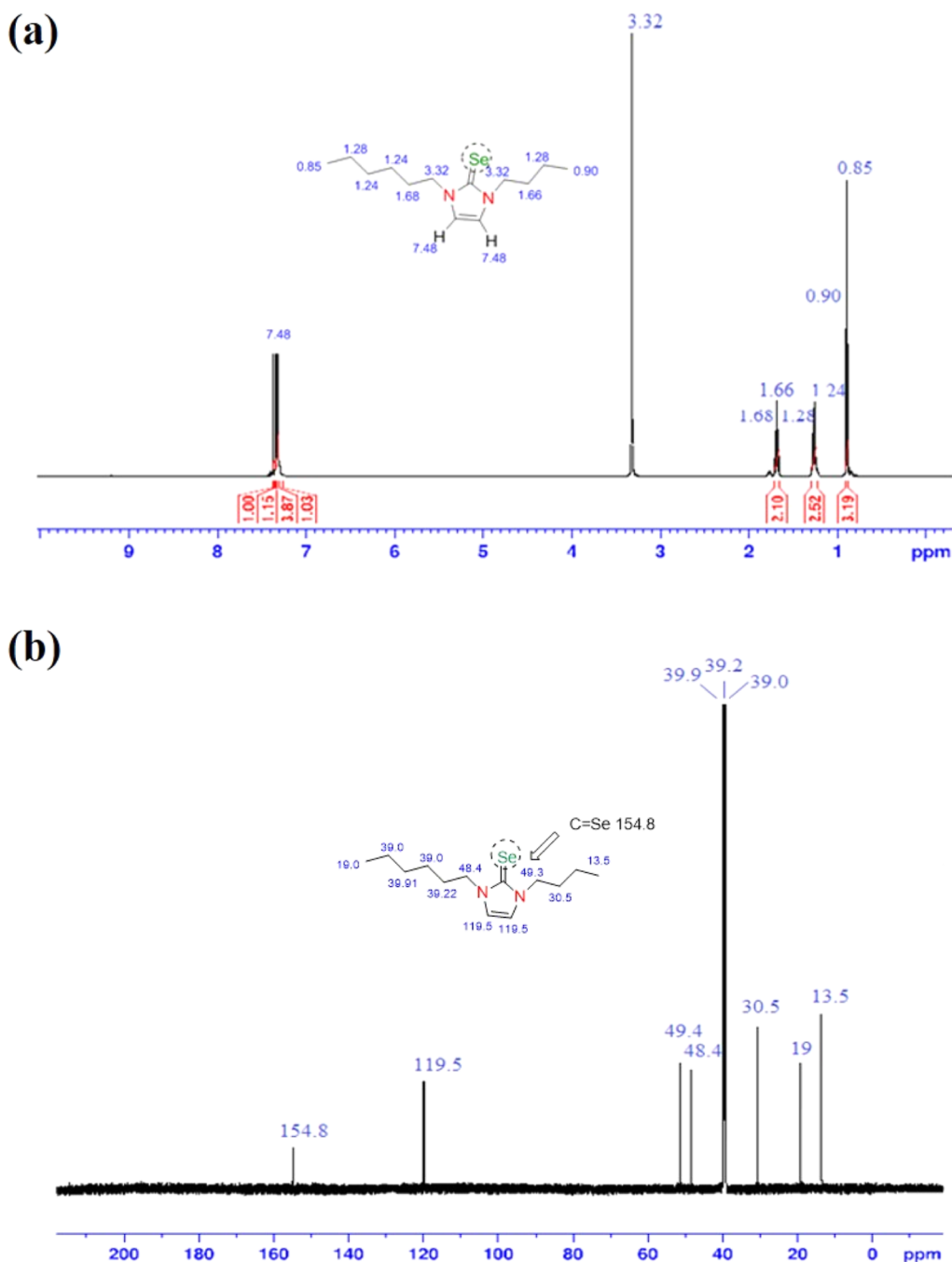
Figure 2. (a) ^{1}H NMR spectra of the Se–NHC adduct (the peak at 9.20 ppm disappears). (b) ^{13}C NMR spectra of the Se–NHC adduct (peak shifted toward the downfield region 154.8 ppm).

can also be used as chemotherapeutic agents because of their high anticancer activity and low toxicity.[10] Selenium, in trace amount, can be used as an antibacterial agent and antifungal agent, making it suitable for medicinal purpose.[11] The above NMR and FT-IR spectra confirm the 2D chemical structure of 1-butyl-3-hexyl-1H-imidazol-2(3H)-selenone having chemical formula $C_{13}H_{24}N_2Se$ which is presented in Figure 3.

2.4. Inhibition Zone Analysis. The bioassay of lab-synthesized organometallic compound against *A. flavus* fungus by the disk diffusion method is indicated in Figure 4 with five zones of inhibition. It can be seen that as the concentration of organometallic compound increases, the size of the zone of inhibition increases. It is found that 300 μM concentration of
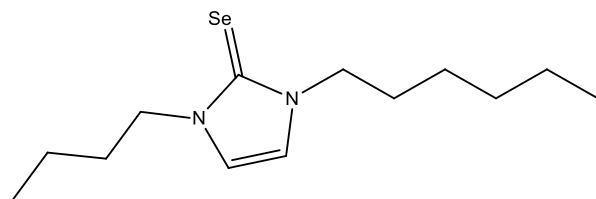

Figure 3. Chemical structure of 1-butyl-3-hexyl-1H-imidazol-2(3H)-selenone.

the Se–NHC complex showed greater inhibition against *A. flavus* as compared to other concentrations (Figure 5).
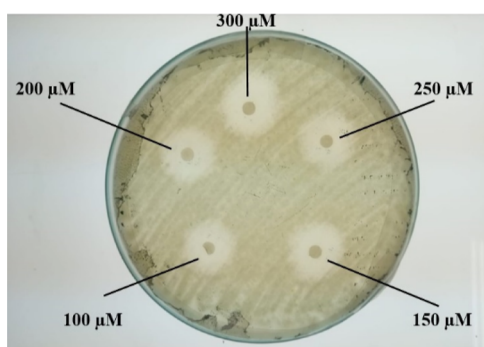
Figure 4. Zone of inhibition analysis to evaluate the antifungal activity of lab-synthesized 1-butyl-3-hexyl-1*H*-imidazol-2(3*H*)-selenone, Se−NHC complex against *A. flavus*.
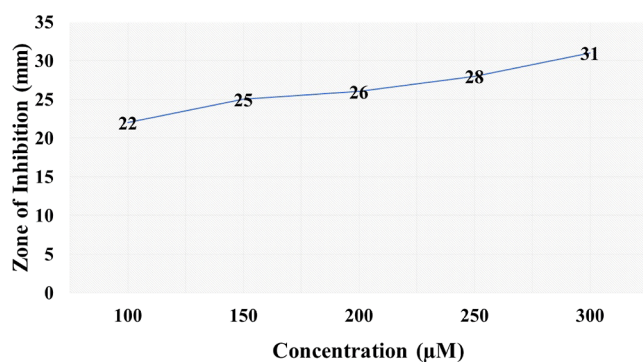

Figure 5. Trend among the two variables, concentration (μM) of the Se−NHC complex, and their zones of inhibition.

2.5. Characterization of Ag-NPs. The characterization of the lab-synthesized Ag-NPs was carried out using transmission electron microscopy (TEM) and scanning electron microscopy (SEM). These NPs have gained extraordinary attention due to their unique chemical and physical properties. By controlling their refractive index, size, and shape, their scattering and absorption properties can be varied. Commonly, the NPs with small size give small enhancement as compared to the NPs with large size.[30,31] NPs with rough surface give greater contribution toward SERS enhancement as compared to the NPs with smooth surface. The characterized NPs were found round with size 65 × 45 nm. The NPs of round geometry and average size were used in various SERS studies, and these NPs give great enhancement for the SERS.[32]

2.6. Mean SERS Spectra. Figure 6a shows the mean SERS spectra of all spectral measurements of *A. flavus* exposed to the Se−NHC complex, N2−N6 (different pellets having different concentrations of organometallic compound), and the unexposed *A. flavus*, N1. Different SERS spectral features distinguishing between exposed and unexposed fungi are identified. The SERS spectral data, which include features that may potentially differentiate the samples, are indicated by solid and dashed lines, and peak assignments of these features has been provided in Table 1. The solid lines are used to label the differentiating SERS bands, while the dashed lines are used to label the intensity-based variations present among the SERS bands. The SERS spectral features that are associated with the biochemical changes related with carbohydrates, proteins, nucleic acids, and lipids produced in the fungal strains due to the exposure of the Se−NHC complex as compared to the unexposed fungal strain of *A. flavus* include 532 cm^{-1} [guanine

(G) (nucleic acids)], 653 cm^{-1} [C−S stretching and C−C twisting (proteins)], 675 cm^{-1} [a ring breathing mode of tyrosine (protein)], 713 cm^{-1} [adenine (nucleic acid)], 722 cm^{-1} [adenine (nucleic acid)], 748 cm^{-1} [adenine (nucleic acid)], 798 cm^{-1} [uracil (RNA)], 818 cm^{-1} [phosphodiester band in DNA and RNA (nucleic acid)], 863 cm^{-1} (carbohydrate), 888 cm^{-1} [C−O−C stretching (carbohydrate)], 949 cm^{-1} [C=C deformation, C−N stretching (protein)], 1000 cm^{-1} [phenylalanine (protein)], 1111 cm^{-1} [bending (C−H) (protein)], 1133 cm^{-1} [=C−O−C= (unsaturated fatty acids in lipids)], 1143 cm^{-1} [C−C and C−O stretching groups for polysaccharides (carbohydrates)], 1170 cm^{-1} [C−O ring, aromatic amino acids (proteins)], 1251 cm^{-1} [amide III (protein)], 1393 cm^{-1} [saccharide (carbohydrate)], 1629 cm^{-1} [amide I (protein)], and 1692 cm^{-1} [COO$^-$ asymmetric stretching (protein)], as mentioned in Table 1.

Figure 6b displays the SERS spectral features that are directly associated with the Se−NHC complex itself including 1325 cm^{-1} [CH$_2$ deformation (Se−NHC complex)], 1408 cm^{-1} [C=C stretching (Se−NHC complex)], 1563 cm^{-1} [CH$_3$ deformation (Se−NHC complex)], and 1591 cm^{-1} [CH$_3$ deformation (Se−NHC complex)].

SERS spectral features that are specifically related to the fungal protein components include 653 cm^{-1} [C−S stretching and C−C twisting (proteins)], 675 cm^{-1} [a ring breathing mode of tyrosine (protein)], 949 cm^{-1} [C=C deformation, C−N stretching (protein)], 1000 cm^{-1} [phenylalanine (protein)], 1111 cm^{-1} [bending (C−H) (protein)], 1170 cm^{-1} [C−O ring, aromatic amino acids (proteins)], 1251 cm^{-1} [amide III (protein)], 1629 cm^{-1} [amide I (protein)], and 1692 cm^{-1} [COO$^-$ asymmetric stretching (protein)]. The decrease in the intensities of the peaks at 653, 1170, 1251, and 1629 cm^{-1} is observed in the Se−NHC complex-exposed fungal samples as compared to unexposed fungal samples. This suggests the formation of protein aggregates within the fungal hyphae which can be an indication of cellular damage which can affect the overall structure and function of the fungal cells.[43] The increase in the intensities of the protein bands at 675, 949, 1000, 1111, and 1692 cm^{-1} is possibly the result of the changes in the protein expression in response to the stress caused by exposure to the Se−NHC complex. This type of compensatory response by the fungal species can be an adaptation mechanism aimed at protecting the cells from further damage. The increase in the amount of several cell wall proteins can help in strengthening the cell wall and providing additional protection to the cells, potentially preventing further damage from the Se−NHC complex. This type of response is a common mechanism observed in cells under stress and can help maintain cellular homeostasis.[44]

In addition to phospholipids, fungal cell membranes also contain other lipids, such as ergosterol, which is unique to fungal cells and plays a key role in maintaining the fluidity and integrity of the cell membrane. The SERS spectral feature that is directly associated with the lipid contents of fungus is observed at 1133 cm^{-1} [=C−O−C= (unsaturated fatty acids in lipids)] having decrease in its intensity. This could indicate a decrease in cell fluidity because of the effect of the antifungal drug on the components of the cell membrane. This, combined with homeostatic pressure, could result in disruptions in the cell membrane.[43]

SERS spectral features observed at 532 cm^{-1} [guanine (G) (nucleic acids)], 713 cm^{-1} [adenine (A) (nucleic acids)], 722
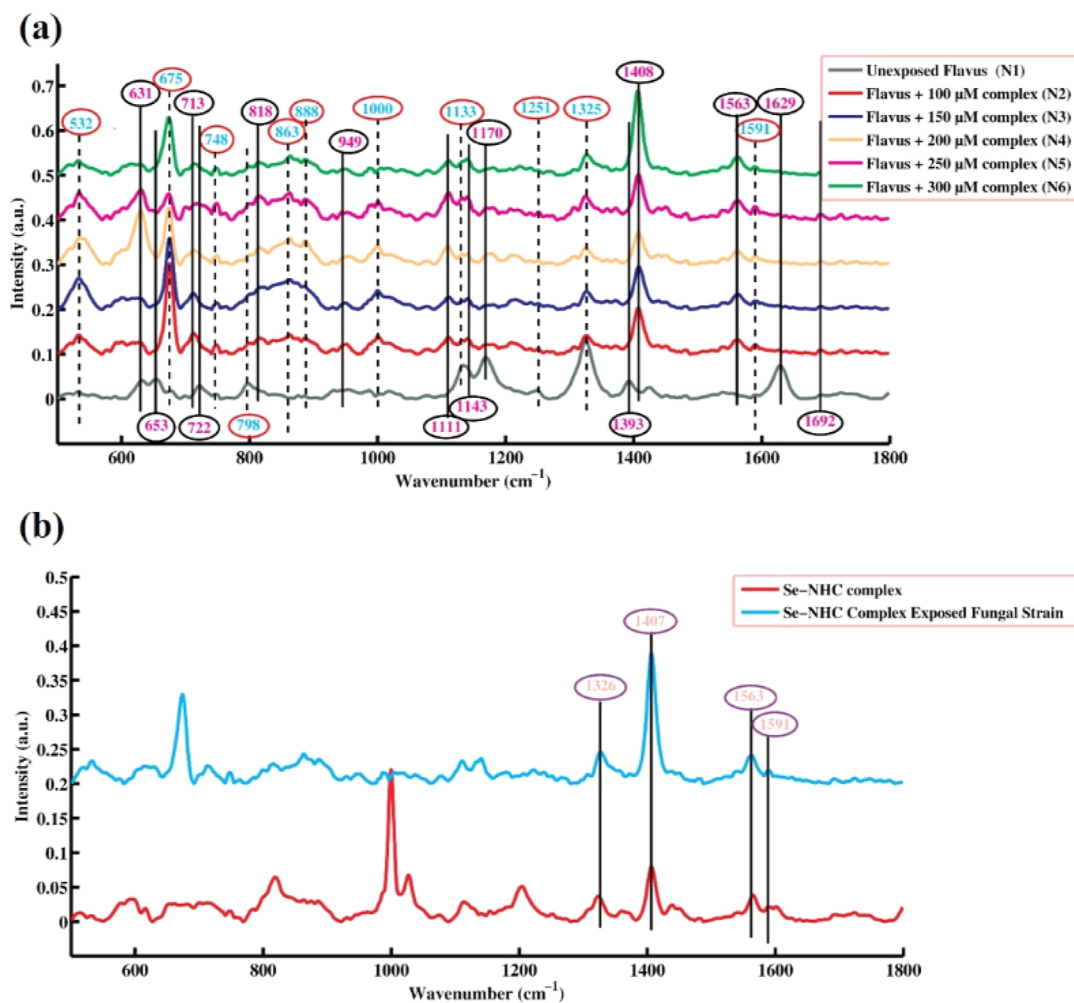
Figure 6. (a) Mean SERS spectra of *A. flavus* samples that were exposed to the Se−NHC complex (N2−N6) and unexposed/control *A. flavus* (N1) and (b) mean SRES spectra of complex exposed fungal strain and Se−NHC complex.

cm^{-1} [adenine (A) (nucleic acids)], 748 cm^{-1} [adenine (nucleic acids)], 798 cm^{-1} [uracil (U) (RNA)], and 818 cm^{-1} [phosphodiester band in DNA and RNA (nucleic acids)] are related with the DNA/RNA fungal content. The bands at 722 and 798 cm^{-1} are related to the PO^{2-} symmetrical stretching and PO^{2-} asymmetrical stretching vibrations of nucleic acids, respectively. These bands provide information about the structure and conformation of the nucleic acids. The decrease in intensity of these bands suggests a change in the structure or conformation of nucleic acids, which could be due to a variety of factors, including changes in gene transcription and/or changes in the interactions between nucleic acids and other cellular components, such as amino acids, which could have significant consequences for cell viability.[43] The bands at 532, 713, 748, and 818 cm^{-1} are related to the stretching vibrations of nucleic acids, including the ribose and phosphate groups. Enhancement in the intensities of these bands would indicate a stress response of the fungal hyphae, which is a response to environmental changes or the presence of an antifungal drug. In response to stress, cells can undergo a variety of changes, including changes in gene expression, metabolism, and structural organization, leading to an increase in the synthesis of DNA and RNA contents.[36]

The SERS peaks at 863 cm^{-1} (carbohydrates), 888 cm^{-1} [C−O−C stretching (carbohydrates)], 1143 cm^{-1} [C−C and

C−O stretching groups for polysaccharides (carbohydrates)], and 1393 cm^{-1} [Saccharide (carbohydrates)] are directly related with the carbohydrate contents of fungus. The intensities of the SERS bands, positioned at 888 and 1143 cm^{-1} related to carbohydrates, are increased. It is possible that the increase in carbohydrates is a response to the inhibitory effect of the antifungal drug as cells may attempt to compensate for the disruptions caused by the drug. This compensatory response would also be due to an increase in the biosynthesis of cellular components, such as cell wall polysaccharides, in an attempt to maintain the structural integrity of the fungal cells.[36]

2.7. Principal Component Analysis. Figure 7 shows the spectral data obtained through SERS of unexposed and complex exposed *A. flavus* fungi that have been distinguished using PCA. These SERS spectral data sets are clearly differentiated by the PCA scatter plot.

Figure 7a shows a PCA scatter plot generated by PCA, which compares the SERS spectral data sets obtained from different concentrations (N2−N6) of the Se−NHC complex-exposed *A. flavus* fungus samples with the unexposed *A. flavus* fungus sample (N1). The PC-1 in the scatter plot effectively differentiates these groups of spectra, accounting for a significant proportion of the explained variance (52.17%), while PC-2 explains 29.55% from the remaining variability.

Table 1. SERS Peak Assignments for SERS Spectra of Fungal Pellets Exposed to the Se−NHC Complex

wavenumber (cm^{-1})	SERS peak assignment	components	refs
532	guanine (G)	nucleic acids	33
653	C−S stretching and C−C twisting	proteins	34
675	the ring breathing of tyrosine	proteins	33
713	adenine (A)	nucleic acids	35
722	adenine (A)	nucleic acids	35
748	adenine (A)	nucleic acids	36
798	uracil (U)	RNA	33
818	phosphodiester band in DNA and RNA	nucleic acids	37
863		carbohydrates	36
888	C−O−C stretching	carbohydrates	36
949	C=C deformation, C−N stretching	proteins	35
1000	phenylalanine	proteins	36
1111	bending (C−H)	proteins	33
1133	=C−O−C=	lipids	35
1143	C−C and C−O stretching groups for polysaccharides	carbohydrates	37
1170	C−O ring, aromatic amino acids	proteins	35
1251	amide III	proteins	36
1325	CH$_2$ deformation	Se−NHC complex	38
1393	saccharide	carbohydrates	39
1408	C=C stretching	Se−NHC complex	40,41
1563	CH$_3$ deformation	Se−NHC complex	41
1591	CH$_3$ deformation	Se−NHC complex	40
1629	amide I	proteins	42
1692	COO$^-$ asymmetric stretching	proteins	39

The loadings of PC-1, which are presented in Figure 7b, provide information based on discriminating biochemical changes in the form of PCA loadings (SERS features) which are responsible for the differentiation of SERS spectra seen in the scatter plot.

The loadings on the positive side of the SERS spectral features in Figure 7b are associated with the Se−NHC complex-exposed fungal samples, while the loadings on the negative side correspond to the unexposed/control *A. flavus* fungus samples. It indicates that the SERS spectral data sets from these groups of samples have distinctive features that can be effectively differentiated using PCA. The positive loadings in SERS spectral features include 532 cm^{-1} [guanine (G) (nucleic acids)], 675 cm^{-1} [a ring breathing mode of tyrosine (protein)], 713 cm^{-1} [adenine (nucleic acids)], 748 cm^{-1} [adenine (nucleic acid)], 818 cm^{-1} [phosphodiester band in DNA and RNA (nucleic acids)], 863 cm^{-1} (carbohydrate), 888 cm^{-1} [C−O−C stretching (carbohydrate)], 1000 cm^{-1} [phenylalanine (protein)], 1111 cm^{-1} [bending (C−H) (protein)], 1408 [CH$_2$, CH$_3$ deformation (lipid)], 1563 cm^{-1} [C−N, C−C stretching and N−H deformation groups of amide II (protein)], and 1591 cm^{-1} [C=C (lipid)]. These SERS spectral features are consistent with the mean plot SERS spectral features, which are presented in Figure 6.

The negative loadings in SERS spectral features include 653 cm^{-1} [C−S stretching and C−C twisting (proteins)], 722 cm^{-1} [adenine (nucleic acid)], 798 cm^{-1} [uracil (RNA)], 949 cm^{-1} [C=C deformation, C−N stretching (protein)], 1133

cm^{-1} [=C−O−C= (unsaturated fatty acids in lipids)], 1143 cm^{-1} [C−C and C−O stretching groups for polysaccharides (carbohydrates)], 1170 cm^{-1} [C−O ring, aromatic amino acids (proteins)], 1251 cm^{-1} [amide III (protein)], 1325 cm^{-1} [amino acids such as L-proline and tryptophan (protein), C−H deformation], 1393 cm^{-1} [saccharide (carbohydrate)], 1629 cm^{-1} [amide I (protein)], and 1692 cm^{-1} [COO$^-$ asymmetric stretching (protein)]. The SERS spectral features mentioned above correspond to the SERS spectral features of the mean plots, which can be visualized in Figure 6.

2.8. Partial Least-Squares Discriminant Analysis (PLS-DA). PCA has been found very effective in achieving differentiation among the SERS spectral data set, as shown in Figure 7. PCA is an unsupervised tool in which group labels are not considered during analysis. As a result, it focuses on the overall variance without necessarily emphasizing the variations related to the treatment groups. However, PLS-DA is a supervised tool in which both the spectral data and the group labels are taken into account, allowing for more precise discrimination between groups. By focusing on the grouping information on the spectra, PLS-DA incorporates class information such as "exposed" and "unexposed" fungal strains to find number of latent variables that maximize the separation between these two classes. Even though PCA visually differentiates the spectral groups in Figure 7, the additional step of PLS-DA allows for a more rigorous statistical analysis, resulting into better accuracy and reliability of the results. PLS-DA focuses on grouping information and incorporation of class information that leads to enhanced differentiation, rigorous statistical analysis, and improved accuracy in classifying distinct groups. PLS-DA, a chemometric method, was also used to analyze these SERS spectra. To perform the differentiation of SERS spectral data sets, the data set was randomly split into a 60% training data set (63 spectra) and a 40% test data set (27 spectra). The Monte Carlo cross-validation (CV) based on the Bayes theorem was used for PLS-DA. To achieve high accuracy, the optimum latent variables (OptLVs) were selected by identifying the variables with the smallest error. 12 optimal latent variables were identified by performing CV, and these were used to train the PLS-DA model with the calibration data set. Since the validation data set was distinct from the trained data set, the trained model was used to check its performance. Figure 8a displays the PLS-DA scores. The PLS-DA model demonstrated a distinct separation between the untreated and treated *A. flavus*, with a sensitivity of 98%, a specificity of 99.7%, and an accuracy of 100%. In-house MATLAB codes were utilized to calculate the precision, sensitivity, specificity, and accuracy of the classification of the SERS spectra for the PLS-DA model. These results suggest that the model is well-suited for this differentiation. The receiver operating characteristic (ROC) curve, which was used to evaluate the performance and effectiveness of the PLS-DA classification model as well as to check the diagnostic ability of SERS, is shown in Figure 8b. The ROC curve was generated by plotting the false positive rate (specificity) against the true positive rate (sensitivity). The AUROC score of 0.87 showed the effectiveness of this model. The PLS-DA classification method was found to be superior to the PCA in terms of its performance in differentiating between treated and untreated *A. flavus* samples. The PLS-DA model classifies the SERS spectra based on biochemical changes in fungi, which result in spectral variations (Table 2).
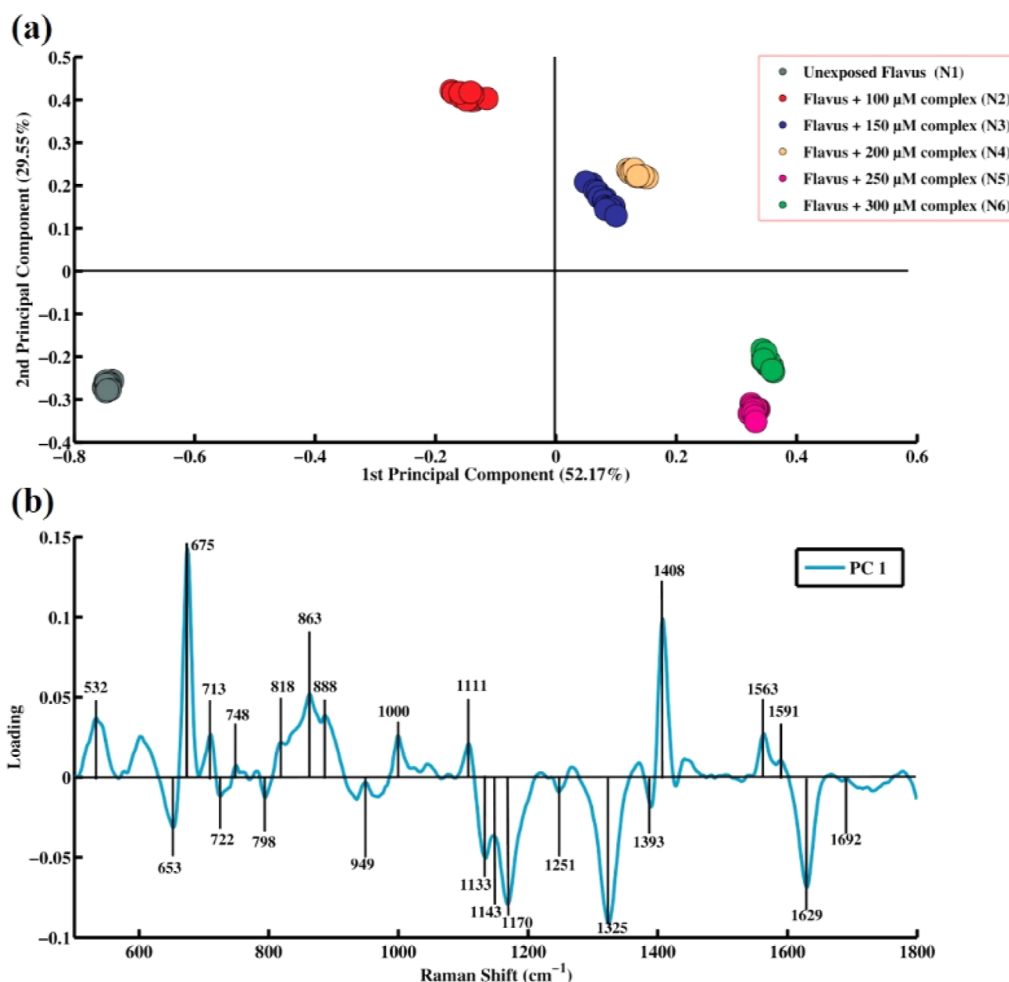
Figure 7. PCA (a) scatter score of SERS spectral data sets of unexposed *A. flavus* (N1) and *A. flavus* fungal strains exposed to various concentrations of the Se−NHC complex (b) loadings of Se−NHC complex exposed *A. flavus* fungal strains versus unexposed *A. flavus* fungus samples.

3. CONCLUSIONS

A Se−NHC complex was synthesized with a high yield, and then, the synthesized Se−NHC complex was characterized using spectroscopic techniques such as FT-IR, ^{1}H NMR, and ^{13}C NMR. The Se−NHC complex demonstrated stability at room temperature both in air and moisture. In vitro disc diffusion assay showed a potential complex as an antifungal agent against *A. flavus*. Surface-enhanced Raman spectroscopy (SERS) can be used as a nondestructive and rapid analytical technique to distinguish between spectral data sets of *A. flavus* fungal samples that have been exposed to Se−NHC complex based on the biochemical changes in their cell walls. This method has the ability to understand the mode of action of the Se−NHC complex against *A. flavus* fungus. The SERS spectra obtained after exposing the fungus to the complex revealed the biochemical changes that occur in the protein and cell membrane components due to growth inhibition. To assess the variability in the SERS spectral data sets, PCA was employed. Additionally, classification of the various spectral data sets was achieved using PLS-DA, resulting in a sensitivity of 98%, specificity of 99.7%, and an accuracy of 100%.

4. MATERIALS AND METHODS

4.1. Synthesis of the Se−NHC Complex. For the process of synthesis, imidazole (1.0 g, 14.7 mmol), dimethyl sulfoxide (20 mL), and KOH (1.23 g, 22.1 mmol) were placed in a round-bottom flask and stirred for 30 min. 1-Bromohexane (0.24 g, 14.7 mmol) was added dropwise, and the temperature of the reaction media was maintained by adding cold water in the reaction mixture. This reaction continued for 4.0 h, and a liquid product 1-hexyl-1*H*-imidazole (N-alkylated compound) having yield 91.5% was obtained. In step-II, N-alkylated compound was dissolved in 1,4-dioxane (25 mL), and 1-bromobutane (0.20 g, 14.7 mmol) was added dropwise in the solution with continuous stirring. The reaction mixture was refluxed for 24 h at 100 °C. The eminent product in from of oily brownish layer obtained which was settled at the bottom of the round-bottom flask. In step-III, 1-butyl-3-hexyl-2,3-dihydro-1*H*-imidazole bromide salt was dissolved in hot distilled water (30 mL), then selenium powder (0.18 g, 2.3 mmol) was blended with K_2CO_3 (0.30 g, 2.2 mmol) and poured into reaction media. The whole reaction mixture was refluxed for 7.5 h, and the product was obtained adhered to the magnetic bar which was separated having yield: 86.8% Scheme 1.

4.2. Antifungal Screening. The disk diffusion method was used to determine the antifungal activity of different
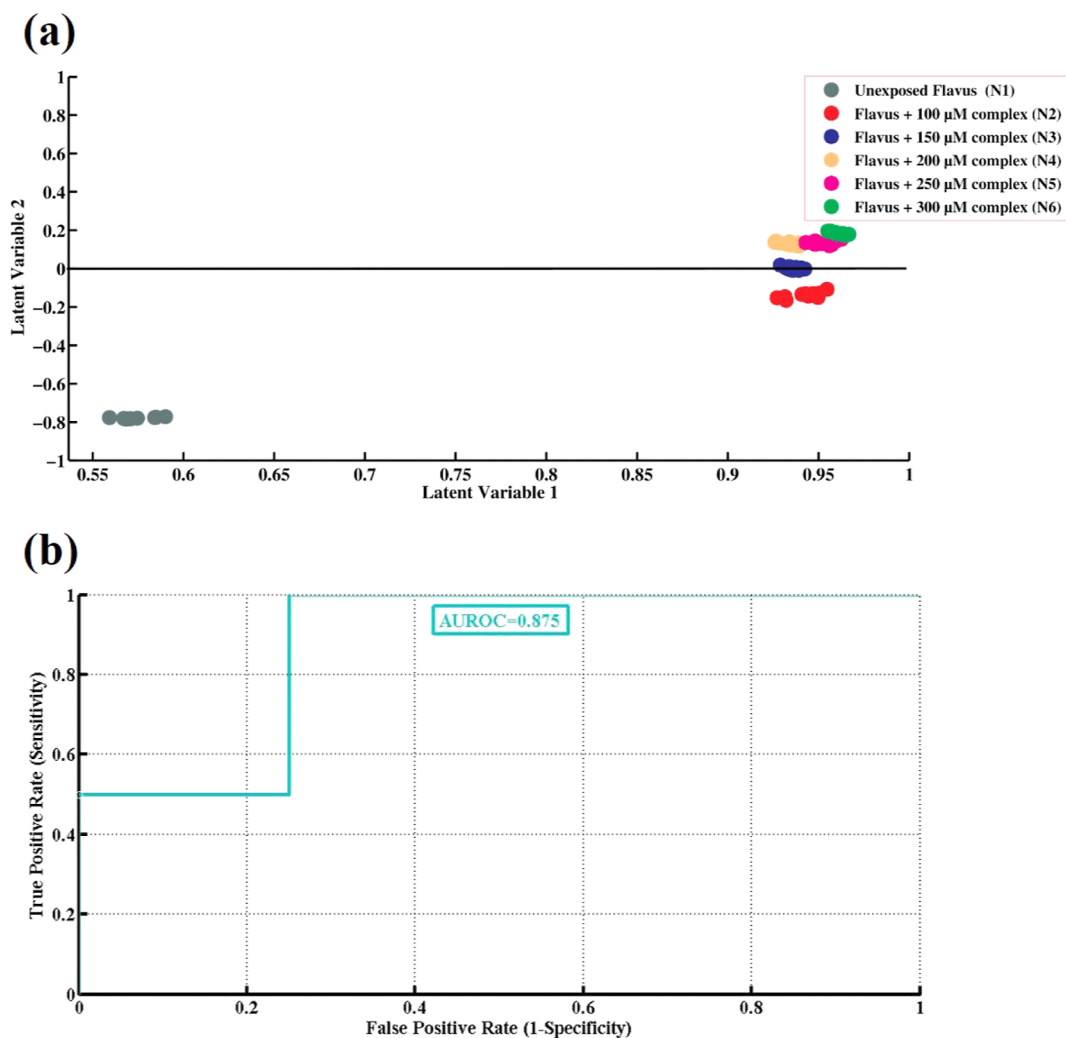
Figure 8. (a) PLS-DA score plot for the test data sets of six samples. (b) ROC curve to evaluate the effectiveness of the PLS-DA model for the various concentrations of the Se−NHC complex.

Table 2. Parameters Evaluated for the PLS-DA Classification Model

parameters	values (%)
sensitivity	98
specificity	99.7
accuracy	100
AUC	87

concentrations of the Se−NHC complex against the fungal pathogen *A. flavus*. In this method, paper disks impregnated with 100 μL of each concentration of the antifungal drug were placed on a culture plate containing the test fungus and then incubated at 37 °C for 48 h. As the antifungal agent diffused into the agar medium surrounding the disk, a zone of inhibition (area where no growth has occurred) around each disk was produced. These inhibition zones were measured which help observe the antifungal activity of different concentrations of drug. In order to do significant, efficient, and more sensitive detection and differentiation analysis of the effect of the antifungal compound on the fungal strain, SERS

Scheme 1. Synthesis of the Se−NHC Complex[a]
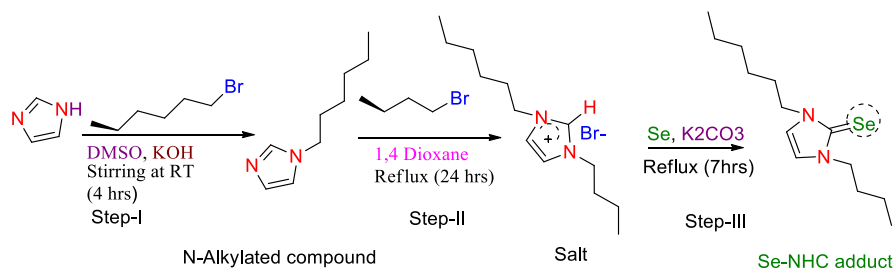
[a]Step-I: synthesis of N-alkylated compound, step-II: synthesis of salt, and tep-III: synthesis of Se-NHC adducts

was employed. SERS significantly detects and differentiates the fungal strain samples that were exposed to the antifungal compound from the other unexposed fungal strain sample.

4.3. Synthesis of Nanoparticles. To synthesize the SERS substrates Ag-NPs, the chemical reduction method was employed using silver nitrate ($AgNO_3$) and trisodium citrate ($Na_3C_6H_5O_7$). Briefly, 17 mg of $AgNO_3$ (precursor) was dissolved in 100 mL of deionized water at 100 °C. Then, 25 mg of $Na_3C_6H_5O_7$ was added as a reducing agent, and the solution was stirred constantly using a magnetic stirrer on a hot plate for approximately an hour. This resulted in gray-colored Ag-NPs. The NPs were further characterized using TEM, SEM, and UV−vis spectrometry.[18,23,34]

4.4. Acquisition of the SERS Spectra. The SERS spectra for each sample were acquired using a pro-785 peak seeker Raman spectrometer (Agiltron, USA). To develop the interaction between the NPs and the sample, 30 μL of fungal pellets suspended in deionized water was incubated with 30 μL of Ag-NPs for 30 min. Then, 30 μL of each incubation mixture was loaded onto an aluminum slide (substrate), and 15 SERS spectra were acquired within the range of 500−1800 cm^{-1} using a 785 nm diode laser. The laser was focused on the sample surface, delivering a laser intensity of 50 mW for 20 s using a 40× objective lens.

4.5. Preprocessing of Raw Spectral Data. The preprocessing of the raw spectral data is mandatory for the purpose of eliminating the noise, correcting the baseline, and smoothing the SERS spectra. All such preprocessing of the raw data was carried out by using house-built codes in MATLAB 7.8.0. version.[45] All raw spectral data were smoothed by employing the Savitzky−Golay (S−G) filter with polynomial order 3 and frame length 13. Rubber band and polynomial methods were used to correct the baseline of the SERS spectra.[46]

4.6. SERS Data Analysis. After preprocessing, all SERS spectral data were further analyzed by using PCA and PLS-DA, chemometric analytical techniques. In exposed and unexposed fungal samples, distinctive SERS characteristic peaks associated with biochemical variations were observed. PCA was applied on the spectral data of pellets of fungal samples to find distinction and variability among these data sets, which are obtained in the form of PCA scatter scores. By transforming correlated variables into a set of linearly uncorrelated variables known as principal components (PCs), PCA helps minimize the dimensionality while maintaining the variance among the data set. The first principal component (PC-1) represents the highest degree of variation in data sets, whereas the second highest degree of variation is explained by second principal component (PC-2).

To simplify the spectral data, the matrix (X) containing the set of spectra was divided into two smaller matrices, including scores (T) and loadings (P). This can be represented by the equation

$$X = TP^T + E$$

where E represents the residual information. Similarities among the SERS spectra of different samples based on their identical molecular properties were revealed by plotting the PC scores.[47] PC loadings are orthogonal variability dimensions that separate different groups of the spectral data across their coefficients.

PLS-DA, a flexible and supervised model, was used to calibrate and validate multivariate differential models by applying them to the spectral data sets for identifying and classifying exposed and unexposed fungal strains. It builds a classification model by using available information on *x*-variables and *y*-variables. The command of randomization was used to mix up the data to avoid bias after combining all of the spectral data into a matrix. The data set was divided into two independent sets including a calibration data set comprising 60% of the data and a validation data set comprising the remaining 40% data. The Monte Carlo CV method was used to determine the optimal number of latent variables (OptLVs) in the data set. Leaving one sample (15 spectra) out, CV was used to develop the PLS-DA model.

Most often, binary classification algorithms are analyzed by using the ROC curve. Binary classification gives four different types of results including true positives (TP), true negatives (TN), false positives (FP), and false negatives (FN).[48] The plot between sensitivity (TP rate) and specificity (FP rate) is known as the ROC curve.[49]

The true positive rate (sensitivity) also known as hit rate and recall can be estimated by[50]

$$sensitivity = TPR$$
$$= \frac{true\ positive\ (TP)}{true\ positive\ (TP) + false\ negative\ (FN)}$$

While the false positive rate (specificity) also known as false alarm rate and inverse recall can be estimated by[50]

$$specificity = FPR$$
$$= \frac{false\ positive\ (FP)}{false\ positive\ (FP) + true\ negative\ (TN)}$$

or[50]

$$specificity = FPR = 1 - sensitivity$$

■ ASSOCIATED CONTENT

ⓢ Supporting Information

The Supporting Information is available free of charge at https://pubs.acs.org/doi/10.1021/acsomega.3c05436.

^{1}H NMR and ^{13}C NMR spectra of Se−NHC salt (PDF)

■ AUTHOR INFORMATION

Corresponding Authors

Haq Nawaz − *Department of Chemistry, University of Agriculture Faisalabad, Faisalabad 38000, Pakistan;* ⊙ orcid.org/0000-0003-2739-4735; Email: haqchemist@yahoo.com

Muhammad Irfan Majeed − *Department of Chemistry, University of Agriculture Faisalabad, Faisalabad 38000, Pakistan;* ⊙ orcid.org/0000-0003-0506-6060; Email: irfan.majeed@uaf.edu.pk

Nosheen Rashid − *Department of Chemistry, University of Education, Faisalabad 38000, Pakistan;* Email: nosheenrasheed@yahoo.com

Authors

Noor ul Huda − *Department of Chemistry, University of Agriculture Faisalabad, Faisalabad 38000, Pakistan*

Muhammad Wasim − *Department of Chemistry, University of Agriculture Faisalabad, Faisalabad 38000, Pakistan*

Muhammad Rizwan Javed − *Department of Bioinformatics and Biotechnology, Government College University Faisalabad (GCUF), Faisalabad 38000, Pakistan*

Muhammad Adnan Iqbal − *Department of Chemistry, University of Agriculture Faisalabad, Faisalabad 38000, Pakistan*

Anam Tariq − *Department of Biochemistry, Government College University Faisalabad (GCUF), Faisalabad 38000, Pakistan*

Ahmad Hassan − *Department of Chemistry, University of Agriculture Faisalabad, Faisalabad 38000, Pakistan*

Muhammad Waseem Akram − *Department of Chemistry, University of Agriculture Faisalabad, Faisalabad 38000, Pakistan*

Faisal Jamil − *Department of Chemistry, University of Agriculture Faisalabad, Faisalabad 38000, Pakistan*

Muhammad Imran − *Department of Chemistry, Faculty of Science, King Khalid University, Abha 61413, Saudi Arabia*

Complete contact information is available at:
https://pubs.acs.org/10.1021/acsomega.3c05436

■ ACKNOWLEDGMENTS

■ REFERENCES

(1) Houšt', J.; Spížek, J.; Havlíček, V. Antifungal drugs. *Metabolites* **2020**, *10* (3), 106.

(2) Rodrigues, M. L.; Albuquerque, P. C. Searching for a change: The need for increased support for public health and research on fungal diseases. *PLoS Neglected Trop. Dis.* **2018**, *12* (6), No. e0006479.

(3) Lin, Y.; Betts, H.; Keller, S.; Cariou, K.; Gasser, G. Recent developments of metal-based compounds against fungal pathogens. *Chem. Soc. Rev.* **2021**, *50* (18), 10346−10402.

(4) Rauseo, A. M.; Coler-Reilly, A.; Larson, L.; Spec, A. Hope on the horizon: novel fungal treatments in development. *Open Forum Infect. Dis.* **2020**, *7*, ofaa016.

(5) Hasim, S.; Coleman, J. J. Targeting the fungal cell wall: current therapies and implications for development of alternative antifungal agents. *Future Med. Chem.* **2019**, *11* (8), 869−883.

(6) Hutchings, M. I.; Truman, A. W.; Wilkinson, B. Antibiotics: past, present and future. *Curr. Opin. Microbiol.* **2019**, *51*, 72−80.

(7) Chohan, Z. H.; Pervez, H.; Khan, K. M.; Supuran, C. T. Organometallic-based antibacterial and antifungal compounds: transition metal complexes of 1, 1′-diacetylferrocene-derived thiocarbohydrazone, carbohydrazone, thiosemicarbazone and semicarbazone. *J. Enzyme Inhib. Med. Chem.* **2005**, *20* (1), 81−89.

(8) Patil, S. A.; Patil, S. A.; Patil, R.; Keri, R. S.; Budagumpi, S.; Balakrishna, G. R.; Tacke, M. N-heterocyclic carbene metal complexes as bio-organometallic antimicrobial and anticancer drugs. *Future Med. Chem.* **2015**, *7* (10), 1305−1333.

(9) Wang, N.; Tan, H.-Y.; Li, S.; Xu, Y.; Guo, W.; Feng, Y. Supplementation of micronutrient selenium in metabolic diseases: its role as an antioxidant. *Oxid. Med. Cell. Longevity* **2017**, *2017*, 1−13.

(10) Kuršvietienė, L.; Mongirdienė, A.; Bernatonienė, J.; Šulinskienė, J.; Stanevičienė, I. Selenium anticancer properties and impact on cellular redox status. *Antioxidants* **2020**, *9* (1), 80.

(11) Satarzadeh, N.; Sadeghi Dousari, A.; Amirheidari, B.; Shakibaie, M.; Ramezani Sarbandi, A.; Forootanfar, H. An insight into biofabrication of selenium nanostructures and their biomedical application. *3 Biotech* **2023**, *13* (3), 79.

(12) Quiroga, E. N.; Sampietro, A. R.; Vattuone, M. A. Screening antifungal activities of selected medicinal plants. *J. Ethnopharmacol.* **2001**, *74* (1), 89−96.

(13) Quiroga, E. N.; Sampietro, D. A.; Soberon, J. R.; Sgariglia, M. A.; Vattuone, M. A. Propolis from the northwest of Argentina as a source of antifungal principles. *J. Appl. Microbiol.* **2006**, *101* (1), 103−110.

(14) Dietvorst, J., An Optofluidic Microwell Structure for the Rapid Determination of the Minimum Inhibitory Concentration (MIC) of Antibiotics. **2022**.

(15) Ge, Y.; Tian, T.; Huang, S.; Wan, F.; Li, J.; Li, S.; Wang, X.; Yang, H.; Hong, L.; Wu, N.; et al. An integrative drug repositioning framework discovered a potential therapeutic agent targeting COVID-19. *Signal Transduction Targeted Ther.* **2021**, *6* (1), 165.

(16) Das, R. S.; Agrawal, Y. Raman spectroscopy: Recent advancements, techniques and applications. *Vib. Spectrosc.* **2011**, *57* (2), 163−176.

(17) Moreira, L. M.; Silveira Jr, L.; Santos, F. V.; Lyon, J. P.; Rocha, R.; Zângaro, R. A.; Villaverde, A. B.; Pacheco, M. T. Raman spectroscopy: A powerful technique for biochemical analysis and diagnosis. *Spectroscopy* **2008**, *22* (1), 1−19.

(18) Saleem, M.; Majeed, M. I.; Nawaz, H.; Iqbal, M. A.; Hassan, A.; Rashid, N.; Tahir, M.; Raza, A.; ul Hassan, H. M.; Sabir, A.; et al. Surface-enhanced Raman spectroscopy for the characterization of the antibacterial properties of imidazole derivatives against bacillus subtilis with principal component analysis and partial least squares-discriminant analysis. *Anal. Lett.* **2022**, *55* (13), 2132−2146.

(19) Arabi, M.; Ostovan, A.; Zhang, Z.; Wang, Y.; Mei, R.; Fu, L.; Wang, X.; Ma, J.; Chen, L. Label-free SERS detection of Raman-Inactive protein biomarkers by Raman reporter indicator: Toward ultrasensitivity and universality. *Biosens. Bioelectron.* **2021**, *174*, 112825.

(20) Jayan, H.; Bhavani Devi, L.; Anandharamakrishnan, C. Nanosensors for Food Contaminant Detection. *Food Nanotechnology*; CRC Press, 2019; pp 309−340..

(21) Khurana, K.; Jaggi, N. Localized surface plasmonic properties of Au and Ag nanoparticles for sensors: A review. *Plasmonics* **2021**, *16* (4), 981−999.

(22) Sharma, B.; Frontiera, R. R.; Henry, A.-I.; Ringe, E.; Van Duyne, R. P. SERS: Materials, applications, and the future. *Mater. Today* **2012**, *15* (1−2), 16−25.

(23) Shakeel, M.; Majeed, M. I.; Nawaz, H.; Rashid, N.; Ali, A.; Haque, A.; Akbar, M. U.; Tahir, M.; Munir, S.; Ali, Z.; et al. Surface-enhanced Raman spectroscopy for the characterization of pellets of biofilm forming bacterial strains of Staphylococcus epidermidis. *Photodiagn. Photodyn. Ther.* **2022**, *40*, 103145.

(24) Fang, H.; Zhang, X.; Zhang, S. J.; Liu, L.; Zhao, Y. M.; Xu, H. J. Ultrasensitive and quantitative detection of paraquat on fruits skins via surface-enhanced Raman spectroscopy. *Sens. Actuators, B* **2015**, *213*, 452−456.

(25) Caro, C.; Castillo, P. M.; Klippstein, R.; Pozo, D.; Zaderenko, A. P. Silver nanoparticles: sensing and imaging applications. *Silver Nanopart.* **2010**, *9S*, 201−224.

(26) Hayat, K.; Shkeel, M.; Iqbal, M. A.; Quah, C. K.; Wong, Q. A.; Nazari V, M.; Ahamed, M. B. K.; Hameed, S. O-Halogen-substituted arene linked selenium-N-heterocyclic carbene compounds induce significant cytotoxicity: Crystal structures and molecular docking studies. *J. Organomet. Chem.* **2023**, *985*, 122593.

(27) Iqbal, M. A.; Haque, R. A.; Ng, W. C.; Hassan, L. E.; Majid, A. M.; Razali, M. R. Green synthesis of mono-and di-selenium-N-heterocyclic carbene adducts: Characterizations, crystal structures and pro-apoptotic activities against human colorectal cancer. *J. Organomet. Chem.* **2016**, *801*, 130−138.

(28) Naz, N.; Saqib, S.; Ashraf, R.; Majeed, M. I.; Iqbal, M. A. Synthesis of new organoselenium compounds: characterization and biological studies. *Maced. J. Chem. Chem. Eng.* **2020**, *39* (1), 1−10.

(29) Ashraf, R.; Khalid, Z.; Sarfraz, A.; Bhatti, H. N.; Iqbal, M. A.; Nazari V, M. Azolium mediated NHeterocyclic carbene selenium adducts: Synthesis, cytotoxicity and molecular docking studies. *J. Mol. Struct.* **2021**, *1241*, 130701.

(30) Cassar, R. N.; Graham, D.; Larmour, I.; Wark, A. W.; Faulds, K. Synthesis of size tunable monodispersed silver nanoparticles and the effect of size on SERS enhancement. *Vib. Spectrosc.* **2014**, *71*, 41−46.

(31) Pustovit, V. N.; Shahbazyan, T. V. Quantum-size effects in SERS from noble-metal nanoparticles. *Microelectron. J.* **2005**, *36* (3−6), 559−563.

(32) Bashir, S.; Nawaz, H.; Irfan Majeed, M.; Mohsin, M.; Nawaz, A.; Rashid, N.; Batool, F.; Akbar, S.; Abubakar, M.; Ahmad, S.; et al. Surface-enhanced Raman spectroscopy for the identification of tigecycline-resistant E. coli strains. *Spectrochim. Acta, Part A* **2021**, *258*, 119831.

(33) Ramirez-Perez, J. C.; A Reis, T.; Olivera, C. L.; Rizzutto, M. A. Impact of silver nanoparticles size on SERS for detection and identification of filamentous fungi. *Spectrochim. Acta, Part A* **2022**, *272*, 120980.

(34) Raza, A.; Parveen, S.; Majeed, M. I.; Nawaz, H.; Javed, M. R.; Iqbal, M. A.; Rashid, N.; Haider, M. Z.; Ali, M. Z.; Sabir, A.; et al. Surface-enhanced Raman spectral characterization of antifungal activity of selenium and zinc based organometallic compounds. *Spectrochim. Acta, Part A* **2023**, *285*, 121903.

(35) Witkowska, E.; Jagielski, T.; Kamińska, A.; Kowalska, A.; Hryncewicz-Gwóźdź, A.; Waluk, J. Detection and identification of human fungal pathogens using surface-enhanced Raman spectroscopy and principal component analysis. *Anal. Methods* **2016**, *8* (48), 8427−8434.

(36) He, L.; Liu, Y.; Mustapha, A.; Lin, M. Antifungal activity of zinc oxide nanoparticles against Botrytis cinerea and Penicillium expansum. *Microbiol. Res.* **2011**, *166* (3), 207−215.

(37) Saif, F.; Yaseen, S.; Alameen, A.; Mane, S.; Undre, P. Identification and characterization of Aspergillus species of fruit rot fungi using microscopy, FT-IR, Raman and UV-Vis spectroscopy. *Spectrochim. Acta, Part A* **2021**, *246*, 119010.

(38) Sheppard, N. Some characteristic frequencies in the Raman spectra of saturated aliphatic hydrocarbons. *J. Chem. Phys.* **1948**, *16* (7), 690−697.

(39) Dina, N. E.; Gherman, A. M. R.; Chiş, V.; Sârbu, C.; Wieser, A.; Bauer, D.; Haisch, C. Characterization of clinically relevant fungi via SERS fingerprinting assisted by novel chemometric models. *Anal. Chem.* **2018**, *90* (4), 2484−2492.

(40) Ashraf, M. N.; Majeed, M. I.; Nawaz, H.; Iqbal, M. A.; Iqbal, J.; Iqbal, N.; Hasan, A.; Rashid, N.; Abubakar, M.; Nawaz, M. Z.; et al. Raman spectroscopic characterization of selenium N-heterocyclic carbene compounds. *Spectrochim. Acta, Part A* **2022**, *270*, 120823.

(41) Ali, S.; Riaz, A.; Majeed, M. I.; Iqbal, M. A.; Bhatti, H. N.; Rashid, N.; Kashif, M.; Tahir, M.; Nasir, S.; Farooq, S.; et al. Raman spectroscopy along with Principal Component Analysis for the confirmation of Silver (I)-N-heterocyclic carbene complex formation. *Spectrochim. Acta, Part A* **2020**, *228*, 117851.

(42) Guo, Z.; Wang, M.; Barimah, A. O.; Chen, Q.; Li, H.; Shi, J.; El-Seedi, H. R.; Zou, X. Label-free surface enhanced Raman scattering spectroscopy for discrimination and detection of dominant apple spoilage fungus. *Int. J. Food Microbiol.* **2021**, *338*, 108990.

(43) Clemente, I.; Aznar, M.; Nerin, C. Raman imaging spectroscopy as a tool to investigate the cell damage on Aspergillus ochraceus caused by an antimicrobial packaging containing benzyl isothiocyanate. *Anal. Chem.* **2016**, *88* (9), 4772−4779.

(44) Víglaš, J.; Olejníková, P. Signalling mechanisms involved in stress response to antifungal drugs. *Res. Microbiol.* **2021**, *172* (1), 103786.

(45) Nawaz, H.; Bonnier, F.; Knief, P.; Howe, O.; Lyng, F. M.; Meade, A. D.; Byrne, H. J. Evaluation of the potential of Raman microspectroscopy for prediction of chemotherapeutic response to cisplatin in lung adenocarcinoma. *Analyst* **2010**, *135* (12), 3070−3076.

(46) Batool, F.; Nawaz, H.; Majeed, M. I.; Rashid, N.; Bashir, S.; Bano, S.; Tahir, F.; Haq, A. u.; Saleem, M.; Nawaz, M. Z.; et al. Surface-enhanced Raman spectral analysis for comparison of PCR products of hepatitis B and hepatitis C. *Photodiagn. Photodyn. Ther.* **2021**, *35*, 102440.

(47) Surmacki, J.; Brozek-Pluska, B.; Kordek, R.; Abramczyk, H. The lipid-reactive oxygen species phenotype of breast cancer. Raman spectroscopy and mapping, PCA and PLSDA for invasive ductal carcinoma and invasive lobular carcinoma. Molecular tumorigenic mechanisms beyond Warburg effect. *Analyst* **2015**, *140* (7), 2121−2133.

(48) Canbek, G.; Sagiroglu, S.; Temizel, T. T.; Baykal, N. In Binary classification performance measures/metrics: A comprehensive visualized roadmap to gain new insights, *2017 International Conference on Computer Science and Engineering (UBMK)*, IEEE: 2017; pp 821−826.

(49) Rosman, A. S.; Korsten, M. A. Application of summary receiver operating characteristics (sROC) analysis to diagnostic clinical testing. *Adv. Med. Sci.* **2007**, *52*, 76.

(50) Fawcett, T. An introduction to ROC analysis. *Pattern Recognit. Lett.* **2006**, *27* (8), 861−874.

■ NOTE ADDED AFTER ASAP PUBLICATION

After this paper was published ASAP September 21, 2023, a change was made to the author order (Muhammad Rizwan Javed was moved from the 6th author to the 5th author). The corrected version was reposted October 3, 2023.